

# TSR Quantum Dots and their Application to Nanometer-size Memory Devices

●Yoshiki Sakuma ●Yuji Awano ●Masashi Shima

(Manuscript received June 30, 1998)

**This paper describes a novel semiconductor quantum dot (QD) grown in a tetrahedral-shaped recess (TSR) formed on a (111)B GaAs substrate from the material science and device application points of view. After describing the fabrication procedure for TSRs, the growth of InGaAs QDs and their optical properties are explained. Then, this paper shows that an indium-rich InGaAs QD is spontaneously formed at the bottom of each TSR. Next, the mechanism of QD formation is discussed in detail. Then, we explain how magneto-photoluminescence experiments have revealed that the QDs have the optical properties peculiar to zero-dimensional confinement. Next, we present experimental results indicating the excellent growth controllability of the QDs. This paper ends with a description of two possible applications of QDs in electronic memory devices.**

## 1. Introduction

Low-dimensional semiconductor nanostructures such as quantum dots (QDs) and wires have attracted much interest during the past two decades.<sup>1-4)</sup> In particular, QDs, the ultimate miniaturized semiconductor structures, in addition to having many practical applications are expected to exhibit some interesting and important phenomena related to the study of fundamental physics. One of the most significant and straightforward features of QDs is that because of their ultra-small size they can be operated with just a few electrons and/or holes.<sup>5)-8)</sup> This is expected to bring the major advantages of enormously high device integration and also ultra-low chip power consumption.<sup>5)</sup> Another attractive feature of QDs is the inherently discrete nature of their energy levels, which are described by the quantum mechanical theory for charged carriers confined in zero-dimensional space. One can apply these QD characteristics to improve the performance of conventional devices and develop novel functional devices which obey a completely different operat-

ing principle from conventional devices.<sup>1),9)</sup>

Several attempts have been made so far to realize QD structures. Among these are dry etching,<sup>10)</sup> selective epitaxy on a masked or patterned substrate,<sup>3),11)-13)</sup> and the self-assembled method.<sup>14)-16)</sup> However, each of these has its own technological drawbacks. The dry etching method sometimes causes severe damage such as defects or contamination to crystals. Selectively-grown dots reported to date are fascinating, but they are difficult to connect to other structures, including electrodes, because the dots are usually formed at convex structures. Furthermore, although the self-assembled dots, derived from the Stranski-Krastanov (S-K) growth mode in large lattice-mismatched systems, are easy to form directly on a wafer surface and can be made highly dense in a self-organized manner, it is generally difficult to precisely control the position, size uniformity, shape, and alloy composition of the QDs. To apply QDs to electronic devices, we must control their alignment in both the horizontal and vertical directions and independently change their size and composition

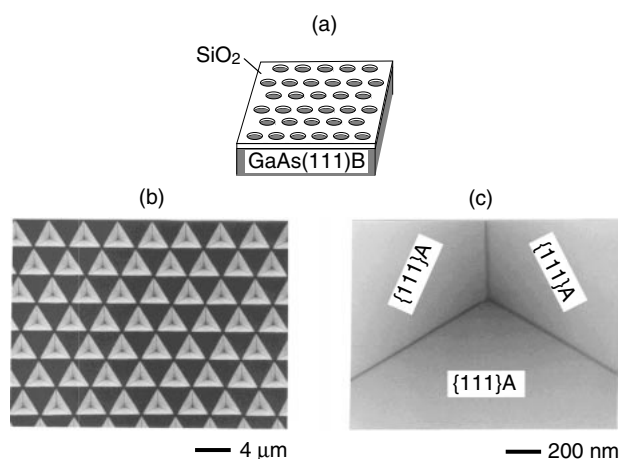


Figure 1  
TSR forming process and SEM plan views of TSRs. (a) Initial GaAs (111)B substrate with 100 nm-thick  $\text{SiO}_2$  patterned mask, (b) SEM picture of TSR array, and (c) magnified SEM view in vicinity of TSR bottom.

to regulate the energy levels. Also, we need to be able to bury the QDs in the host semiconductor materials to easily achieve electrical access to the dots.

To meet these requirements, we have proposed a novel QD structure using tetrahedral-shaped recesses (TSRs), *i.e.*, inverted triangular pyramids formed on a (111)B-oriented substrate.<sup>17),18)</sup> In this article, we describe the procedure for fabricating InGaAs QDs on a TSR-formed substrate and their optical properties, including magneto photoluminescence. Then, we discuss the growth mechanism of a QD formed at the bottom of a TSR. Furthermore, we report on the ability to change the energy levels through size and composition control of the dots during growth. Our goal is to apply the TSR structure to highly-integrated electronic memory devices. Therefore, we also report on some candidate memory devices, and present our preliminary experimental results.

## 2. TSR Quantum Dots

### 2.1 TSR fabrication

Figure 1 shows the process for fabricating TSRs. After forming a  $\text{SiO}_2$  mask having circular openings on a Cr-O doped, semi-insulating (111)B-GaAs substrate, we made TSRs by etching the

substrate with an anisotropic wet chemical etchant; namely, 0.5%  $\text{Br}_2$ -ethanol solution. Each TSR consisted of three equivalent {111}A side facets that appeared owing to the extremely slow etching rate.<sup>19)</sup> An array of TSRs was fabricated on a  $2 \times 2$  mm area of a substrate. Typically, the length of each TSR side at the substrate surface was about 3  $\mu\text{m}$  and the distance between TSRs was 4  $\mu\text{m}$ . Observation by highly-resolved scanning electron microscope (SEM) showed that the {111}A facets were very smooth and the bottom of every recess was sharp and had the same shape. Note that the regular shape of the recess after etching was due to the zinc-blend-type crystallographic characteristics and does not depend on the shape of the initial mask openings. Thus, this TSR formation might be classified as a self-organized process.

### 2.2 TSR-QD formation and optical properties

Using the recessed substrates, we found that InGaAs QDs are easily and successfully formed at the bottom of the TSRs. We grew a GaAs/InGaAs/GaAs heterostructure inside the TSRs using low-pressure metalorganic chemical vapor deposition (MOCVD), as illustrated in Figure 2(a). Growth was performed on the TSR-formed substrates at a temperature of 600°C and a pressure of 50 Torr, without removing the  $\text{SiO}_2$  mask. Trimethylgallium (TMGa), trimethylindium (TMIn), and  $\text{AsH}_3$  were employed as sources. The TMGa was kept at -10°C, and the  $\text{H}_2$  flow rate through the TMGa bubbler was 5 standard cubic centimeters per minute (sccm). The TMIn container was kept at 13.5°C. We made several samples by changing the TMIn flow rates and the growth time for the InGaAs layer. The flow rate of pure (100%)  $\text{AsH}_3$  was always 20 sccm. The total flow rate in the reactor was 2,000 sccm. For all samples, the thickness of buffer and cap GaAs was 100 nm and 150 nm, respectively. Here, the thickness was defined along the normal direction at the {111}A side facets. Under these growth con-

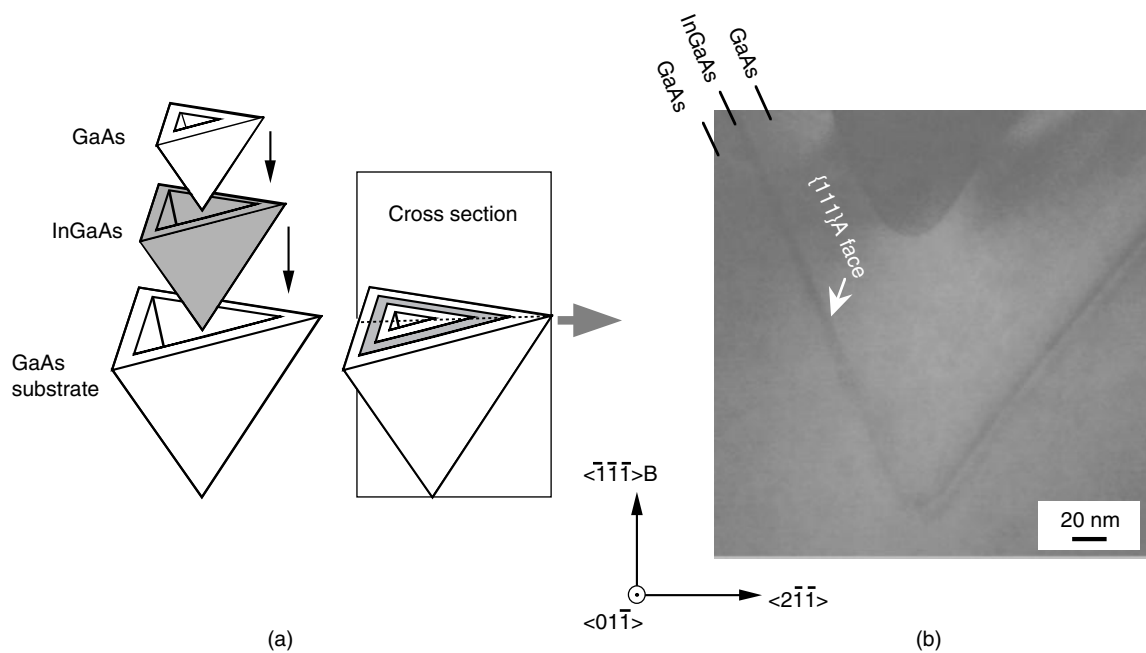


Figure 2  
(a) GaAs/InGaAs/GaAs growth inside TSR, and (b) cross-sectional TEM image.

ditions, we confirmed by SEM that either the GaAs or InGaAs layer had an almost uniform thickness profile on the {111}A faces. In addition, there was no deposition on the mask because of the perfect selective area epitaxy.

Figure 2(b) shows a cross-sectional transmission electron microscope (TEM) image of a sample on which 2.5 nm-thick InGaAs quantum wells (QWs) were grown at {111}A sidewalls under a TMI flow rate of 50 sccm. It is clear that InGaAs was grown at a uniform thickness over the {111}A sidewall of the TSR. In other words, unlike the reported quantum wires grown in the V-grooves formed on (001) substrates,<sup>2),4),20)</sup> we did not observe a growth rate enhancement in the vicinity of the TSR bottom under our growth conditions.

Interestingly, despite the uniform InGaAs thickness, we found two peaks in the low-temperature photoluminescence (PL) spectrum. **Figure 3(a)** shows the PL spectrum at 5 K of the sample shown in Figure 2(b). We observed two distinct

emission peaks: one at 1.45 eV and another at 1.48 eV. The corresponding monochromatic cathodoluminescence (CL) images are shown in Figure 3(b). These plan views of CL images indicate that the emission at 1.45 eV comes from the TSR bottoms and the emission at 1.48 eV comes from the sidewalls. Direct evidence that the luminescence of the lower energy exhibits the properties peculiar to real QDs can be obtained from the magneto-PL studies, as explained in a later section. The results in Figure 3 imply that InGaAs QDs are spontaneously formed at the bottom of every TSR, while the QWs are formed at the sidewalls.

We compared the optical property of the QD emission peak with that of QWs by studying the dependence of CL spectra on the excitation power of the electron beam. Here, we studied the CL from only one TSR structure because we can easily select one from among the many TSRs by narrowing the scanning area of the electron beam on the sample in the CL apparatus.<sup>21)</sup> The results are shown in **Figure 4** for a sample InGaAs QW

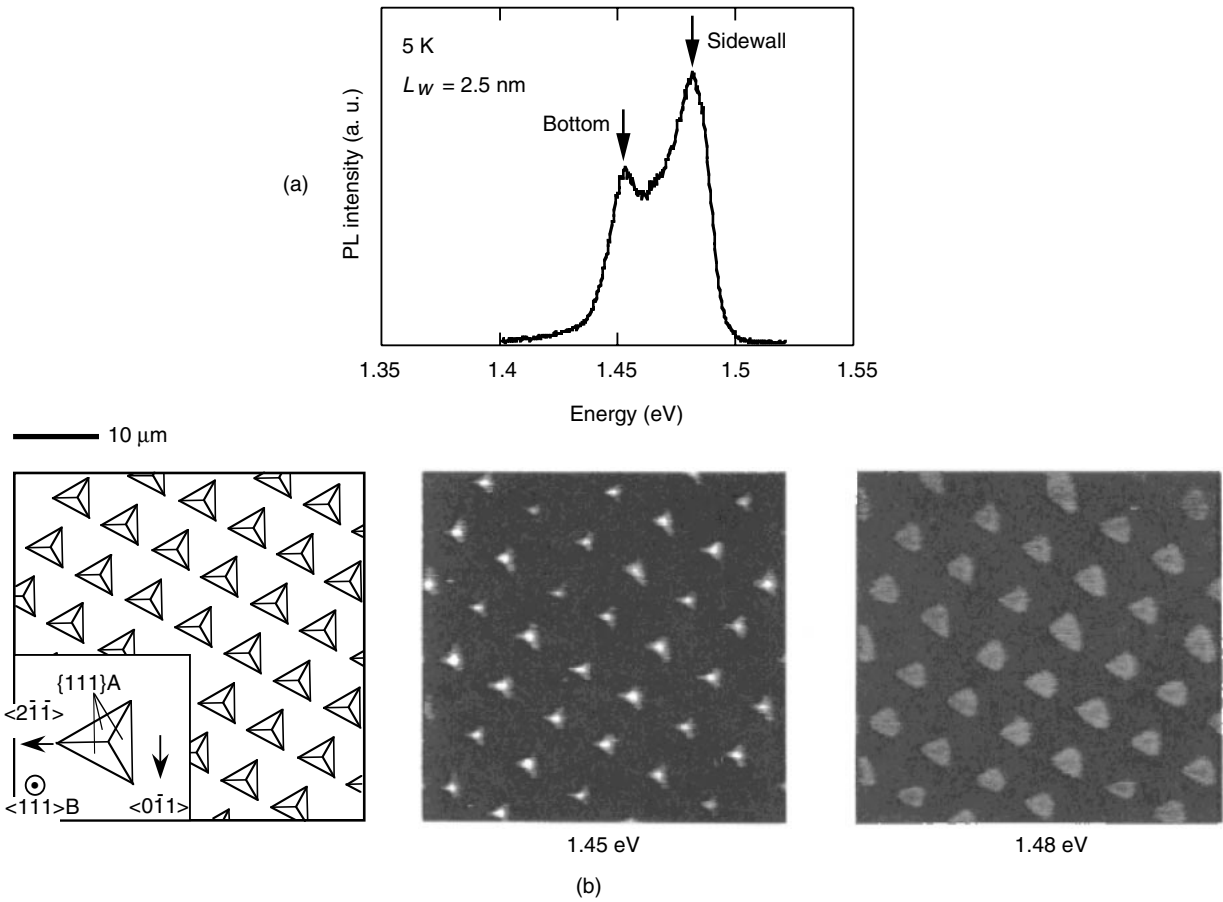


Figure 3 (a) PL spectrum at 5 K and (b) monochromatic CL plan views. Diagram on left shows arrangement of TSRs.

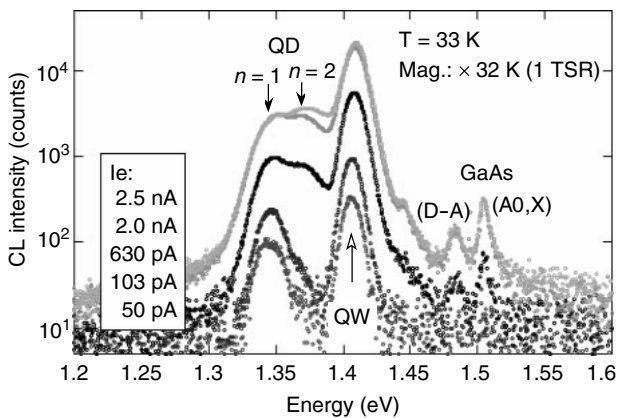


Figure 4 CL spectra at 33 K of single TSR taken at various electron beam currents.

with a width,  $L_w$ , of 5 nm, that was grown under a TMIIn flow rate of 100 sccm. The level of emission current from the electron gun was varied to change the excitation intensity and the acceleration voltage was kept constant at 5 keV. Again, we observed two distinct peaks in the CL spectrum of the lowest excitation level: one from the QD at 1.34 eV and the other from the QWs at 1.41 eV. As the excitation power was increased, the intensity of the QD peak tended to saturate and a new peak appeared at 1.38 eV. The 1.34 eV peak corresponds to the ground state emission of the QD, and the peak at 1.38 eV is from the 1st excited state. This change in the spectra might be due to so-called band filling, or more strictly speaking, due to the state filling phenomena in the dot. At the same time, however, no band-filling was ob-

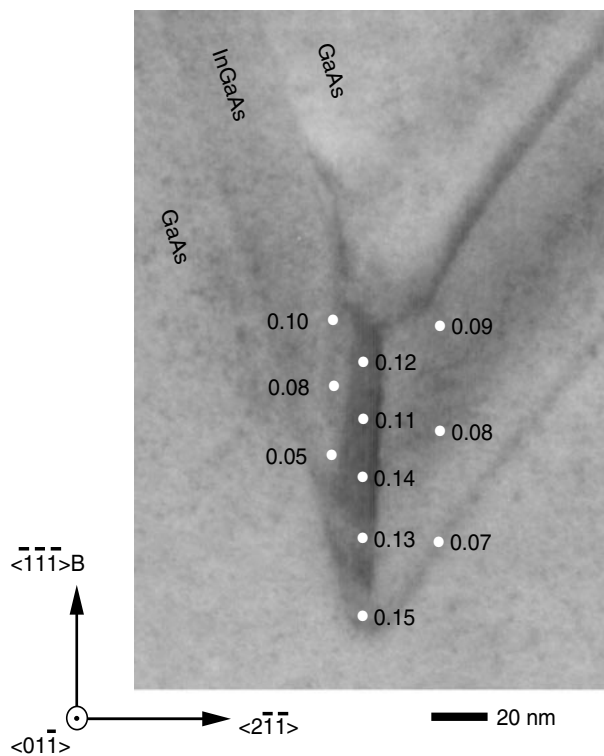


Figure 5  
Cross-sectional TEM image of sample with rather thick InGaAs. Numbers indicate In content of InGaAs near TSR bottom.

served for the QW peak; the peak position of the QW does not shift so much and its intensity increases almost linearly with the power. The fact that the band filling of the QD occurs at a much lower excitation power compared with the QWs on the TSR sidewalls implies that the QD contains only a small number of energy states, suggesting a small size (or volume) QD.

### 2.3 Growth mechanism

From the scientific perspective, it is very important to reveal the self-forming mechanism of a QD at the TSR bottom. Also, from the technical perspective, clarifying the growth mechanism will be useful for improving the growth process of this TSR-QD and for providing a clue to help us exploit the new QD fabrication technique.

Figure 5 shows a  $(01\bar{1})$  cross-sectional TEM photograph and the indium (In) composition near the bottom of a TSR in which a GaAs/InGaAs/

GaAs heterostructure was grown. The composition was evaluated by energy dispersive X-ray diffraction (EDX) in the TEM apparatus. The spatial resolution of the incident electron beam for EDX analysis was about 1 to 2 nm. In this sample, the  $L_w$  of the InGaAs layer at the  $\{111\}A$  faces was intended to be as thick as 50 nm, much thicker than that of the normal QD samples, so that we could clearly observe the spatial distribution of the composition of ternary alloy. We found that a pillar-shaped nanostructure with a dark contrast grew from the  $(111)B$  bottom of the TSR, and that the region has an In-rich chemical composition. It is difficult to estimate the absolute value of In composition because the TSR bottom is surrounded by bulk GaAs in the TEM specimen. As a result, it should be noted that the observed In compositions are only relative values. The figure shows that the width or diameter of the dark contrast region is 10 to 15 nm, which is small enough to accomplish the quantum confinement of carriers in the horizontal direction. Therefore, the In-rich region will act as a QD when the height of the region is small enough to cause a quantum-confined effect. Thus, the growth mechanism of TSR-QD formation is due not to a strain-induced three-dimensional (3D) growth such as S-K mode growth, but to the compositional nonuniformity of the InGaAs layer in the TSR. The In-rich InGaAs QD is spontaneously formed at the TSR bottom, while an In-poor InGaAs QW is formed at the  $\{111\}A$  sidewalls. The results from structural analysis agree well with the PL and CL results in Figure 3 because the QD peak is observed at a lower energy than the QW emission energy.

Figure 6 shows an ideal crystallographic structure of a TSR as viewed from the top (a) and from the  $(01\bar{1})$  cross section (b). It is assumed that the GaAs surface is As-terminated. There are three kinds of segments inside the TSR which have specific configurations in the surface bonds. The three equivalent sidewalls are  $\{111\}A$ . The three valleys crossing the two  $\{111\}A$  faces have a  $\{100\}$ -like bond configuration. The bottom, cross-

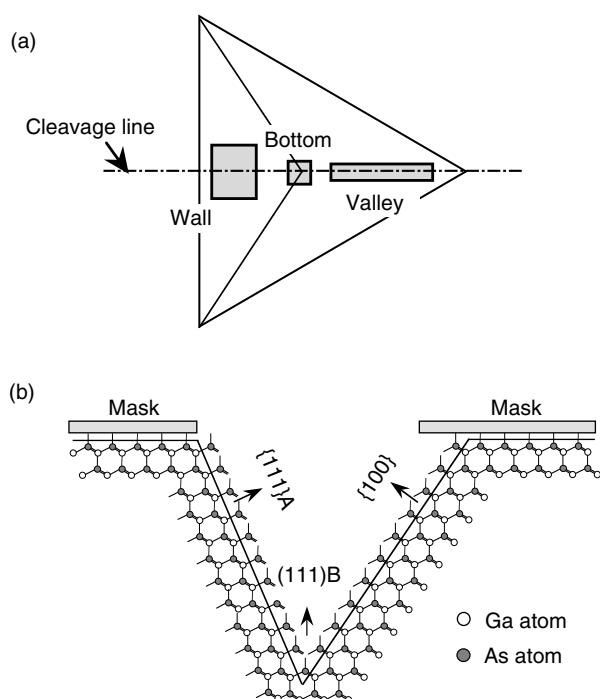


Figure 6  
Crystallographic structure of TSR. (a) Simple top view, and (b) ball and stick model of cross section when TSR is cleaved at center line.

ing the three  $\{111\}$ A faces, has a  $(111)$ B-like bond configuration. We speculate that on growing InGaAs in a TSR using MOCVD, the chemical composition of the InGaAs layer will be strongly affected by these local crystallographic orientations, leading to different surface reaction kinetics.

To confirm this hypothesis, we studied the composition of InGaAs epilayers grown separately on planar (100), (111)A, and (111)B-oriented GaAs substrates. The growth conditions were the same as those employed for the TSR-QDs shown in Figure 5. The InGaAs growth thickness was from 70 to 100 nm. **Table 1** summarizes the In composition of the InGaAs epitaxial layers analyzed by Auger electron microscopy (AES) and the surface morphologies. The results clearly indicate that the In composition is largest on the (111)B substrate. Although there is only a small change in the composition between (100) and (111)A substrates, it is unclear whether the discrepancy is significant. It is obvious that the en-

Table 1  
Indium compositions and surface morphologies of InGaAs grown on substrates of different orientations.

Surface index	$x_{\text{In}}$	Morphology
(100)	0.12*	
(111)A	0.14	
(111)B	0.36	

\*calibrated by XRD

hanced In composition at (111)B is caused by the differences in InGaAs growth kinetics among these orientations because the surface reactions play a crucial role in MOCVD. According to similar experimental results reported elsewhere,<sup>22),23)</sup> the In-rich composition of the InGaAs layer on (111)B is due to suppressed Ga atom incorporation into the surface, rather than increased In atom incorporation. It has also been reported that the probability of In incorporation is not much affected by the surface orientations.<sup>22)</sup> In other reports, the inhibition of Ga adsorption on (111)B GaAs has been observed during GaAs homoepitaxial growth in both molecular beam epitaxy (MBE) under As-rich growth conditions and MOCVD.<sup>24),25)</sup> It is believed that the excessively adsorbed As atoms form chemically stable trimer structures on the GaAs (111)B, and this specific As-rich reconstructed surface, recognized as  $(2 \times 2)$  reconstruction in the case of MBE, deactivates the growth reactions between the surface As and the incoming Ga species.<sup>26)</sup> This phenomena might be related to the growth of In-rich InGaAs at (111)B GaAs, as observed in our experiments.

Referring again to the illustration of Figure 6,

we can apply the results of Table 1 to the self-forming mechanism of TSR-QDs. As explained earlier, the TSR bottom has a (111)B-like bond configuration. Therefore, on growing InGaAs, the In-rich region is grown spontaneously at the bottom. Unlike the ideal picture shown in Figure 6, the bottom of the TSR is actually not acute in atomic dimensions, and instead has a finite flat area of (111)B orientation under the growth conditions. This area limits the horizontal size of the In-rich QD. On the basis of this growth mechanism, the In-rich region becomes a QD when we grow thin InGaAs. On the other hand, when we grow a rather thick InGaAs layer, the In-rich region is grown upwards automatically and becomes a vertical quantum dash or a wire, as in Figure 5. Thus, we can control the vertical QD size through the InGaAs growth thickness. Details are given in a later section.

## 2.4 Magneto-PL studies

Although the above-mentioned TEM result and the state-filling effect in luminescence strongly support the formation of QDs at the bottom of TSR structures, they are only indirect evidence. Therefore, we have to acquire direct evidence of zero-dimensional carrier confinement in a QD. In addition, we need to clarify the extent of the wavefunction of a TSR-QD, particularly in the horizontal direction. We performed magneto-PL studies on our TSR sample under high-intensity magnetic fields, because this directly provides us with the above-mentioned evidence.

We collaborated with the group of Professor N. Miura at the Institute of Solid State Physics, the University of Tokyo, where we had access to pulsed, high-intensity magnetic fields of up to 40 tesla (T). We studied the magneto-PL at 50 K in both the Faraday ( $\mathbf{B} // z \perp \mathbf{E}$ ) and Voigt ( $\mathbf{B} \perp z \perp \mathbf{E}$ ) configurations; where  $\mathbf{B}$ ,  $z$ , and  $\mathbf{E}$  are the magnetic field vector, the direction along  $\langle 111 \rangle_B$ , and the electric field vector of luminescent light, respectively. The PL spectra were gathered from numerous TSRs within a 1 mm $\phi$  area using an opti-

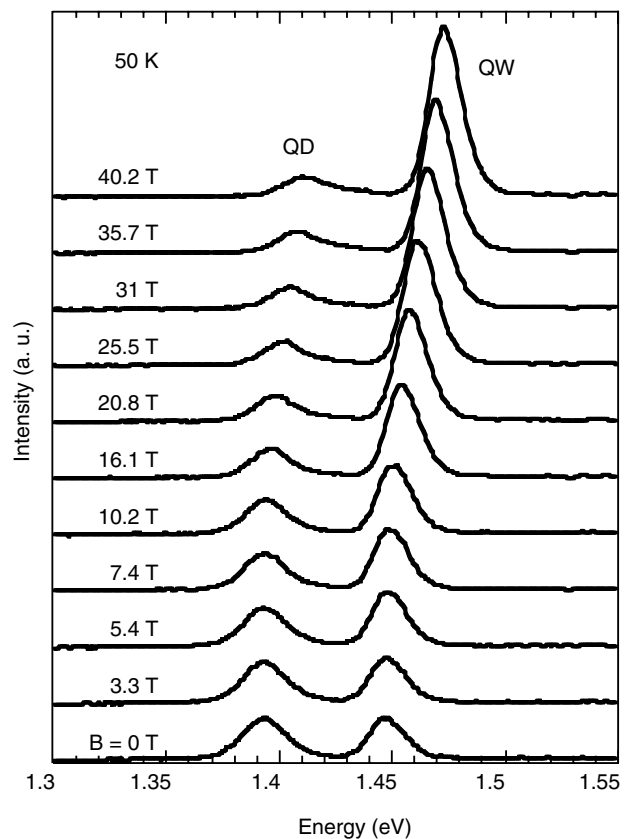


Figure 7  
PL spectra measured at various magnetic fields in Faraday configuration.

cal fiber scope, and the dispersed light was detected by an optical multichannel analyzer (Si CCD) system combined with a single monochromator. The 488 nm line of an Ar<sup>+</sup> laser was used as an excitation source.

The evaluated sample was designed so that the width of the InGaAs QW,  $L_w$ , was 5 nm at the sidewalls. From the geometrical relationship, the height of the QD region,  $h_d$ , was 15 nm. The indium content of InGaAs is proportional to the H<sub>2</sub> flow rate through the TMIn container, which was 100 sccm. **Figure 7** shows PL spectra under various magnetic fields in the Faraday configuration with  $\mathbf{B}$  parallel to the  $z$ , *i.e.*  $\langle 111 \rangle_B$ , direction. Both the QW and QD peaks shift diamagnetically to the higher energy side as the magnetic field intensity increases. Note that increasing the field intensity decreases the QD peak and increases the QW peak. This phenomenon is related to the dy-

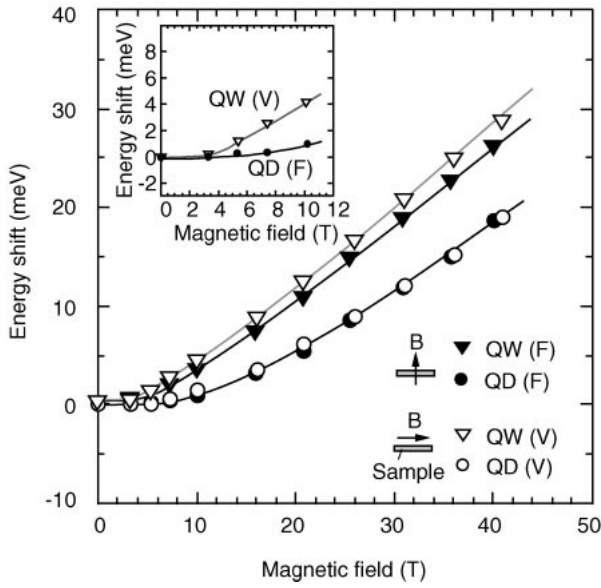


Figure 8 Energy shifts of PL peaks as a function of applied magnetic field. F and V represent Faraday and Voigt configuration, respectively.

namics of photo-generated carriers during the recombination process. We believe that most of the electrons and holes emitting the QDs luminescence are generated in bulk GaAs and are supplied to In-rich InGaAs QDs at the bottoms by way of the In-poor QWs at the sidewalls. When a magnetic field is applied, cyclotronic motion of carriers occurs at the QWs. As a result, the radiative recombination probability in QWs increases due to the shrinkage of the excitonic wavefunction, leading to an enhanced QW PL intensity.<sup>12)</sup> Hence, the number of diffused carriers from the QWs increases the QDs is decreased by the application of magnetic fields, resulting in a decreased QD luminescence intensity.

**Figure 8** shows the diamagnetic shifts of the two emission peaks for magnetic fields of up to 40 T. The inset shows the shifts for lower intensities in greater detail. Compared to the energy shifts of the sidewall QW, the QD energy shifts are clearly smaller in both the Faraday and Voigt configurations. This suggests that the carriers are localized in the TSR QDs. We did not observe any significant difference in the QD energy shifts between the Faraday and Voigt configurations. This

means that the carriers, or excitons, are isotropically confined in the TSR-QD of this design. On the other hand, the QW energy shifts are larger in the Voigt configuration than in the Faraday case, especially in the high magnetic field region where the energy shifts are dominated by the Landau shift. This is due to the two-dimensional (2D) characteristics of the excitons confined at the sidewall QWs. For a QW, in general, a larger diamagnetic shift is observed when the magnetic field is perpendicular to the heterointerfaces.<sup>27),28)</sup> This is because carriers can move freely along the QW plane but are structurally restricted from moving perpendicular to the interfaces. Since the three {111}A facets are steeply inclined at an angle of 70.5° from the <111>B direction, the component of the magnetic field that is perpendicular to the QW plane is larger in the Voigt configuration than in the Faraday case.

To estimate the extent of the wavefunction of the confined carriers, we analyzed the data of the diamagnetic shifts on the basis of the hydrogen-like exciton model.<sup>29)</sup> Generally, under low magnetic field conditions, the exciton Bohr radius,  $a^*$ , is much smaller than the magnetic length  $l_c = \left(\frac{\hbar}{eB}\right)^{\frac{1}{2}}$ , where  $\hbar$ ,  $\epsilon$ , and  $e$  are Planck's constant, the dielectric constant, and the electron charge, respectively. In this case, we can treat the magnetic field  $B$  as a small perturbation. As a result, the diamagnetic energy shift shows the following quadratic dependence on the magnetic field:

$$\Delta E_i = \frac{4\pi\hbar^4\epsilon^2}{e^2\mu\mu_j\mu_k} B_i^2 = \beta B_i^2, \quad (i, j, k = x, y, z) \quad (1),$$

where  $\beta$  is the diamagnetic coefficient. The exciton reduced mass,  $\mu$ , is defined as:

$$\frac{1}{\mu} = \frac{1}{3} \left( \frac{1}{\mu_x} + \frac{1}{\mu_y} + \frac{1}{\mu_z} \right) \quad (2),$$

where  $\mu_x, \mu_y, \mu_z$  are the anisotropic exciton reduced masses. Since we assume a columnar shape in our TSR QDs, we use  $\mu_x = \mu_y = \mu_{xy}$ . The anisotropic exciton Bohr radius,  $a^*_{i}$ , is expressed as:

$$\alpha^*_i = \frac{4\pi\hbar^2\varepsilon}{e^2\mu_i}, \quad (i = x, y, z) \quad (3).$$

From the QD energy shift data in Figure 8, we can deduce that  $\beta$  is about  $12 \mu\text{eV}/\text{T}^2$  at fields lower than 10 T with  $lc = 8.1 \text{ nm}$ . Since the excitons in the QD of the above sample are almost isotropic, the Bohr radius is estimated to be about 5.8 nm. Here, we used a GaAs dielectric constant of  $\varepsilon = 13.1\varepsilon_0$  instead of the value for the InGaAs of ambiguous In content, where  $\varepsilon_0$  is the dielectric constant of a vacuum. We believe that the error is within several percent because the In content of InGaAs is small. To obtain an accurate Bohr radius and the anisotropy of excitons at the sidewalls of QWs, we must separate the applied magnetic field into one component that is perpendicular to the QW plane and one component that is parallel to it. For simplicity, however, we calculated the effective exciton Bohr radius,  $a^*_{\text{eff}}$ , from the low-field data of the Voigt configuration. The effective two dimensional exciton radius,  $a^*_{\text{eff}}$ , obtained for a  $\beta$  value of  $41 \mu\text{eV}/\text{T}^2$  is 8.6 nm at the sidewall InGaAs quantum well. It is reasonable that the Bohr radius of the excitons in a typical TSR-QD is smaller than the effective exciton radius of the sidewall QW, and is also much smaller than the calculated 3D exciton radius of 11.8 nm in bulk GaAs.<sup>29)</sup> Thus, zero-dimensional carrier confinement in the TSR-QD was confirmed from the magneto-PL experiments.

### 2.5 Growth control of TSR-QDs

Unlike the case in the self-assembled QD technique, in conventional photo or electron-beam lithography, we can control the location of TSR-QDs on the surface by precisely positioning the mask openings. However, we need to improve the artificial growth control before we can use the TSR-QDs in practical devices. That is, we need to be able to control the strength of zero-dimensional quantum confinement by regulating the size and chemical composition of the TSR-QDs and we must find a way to stack (vertically align) the dots.

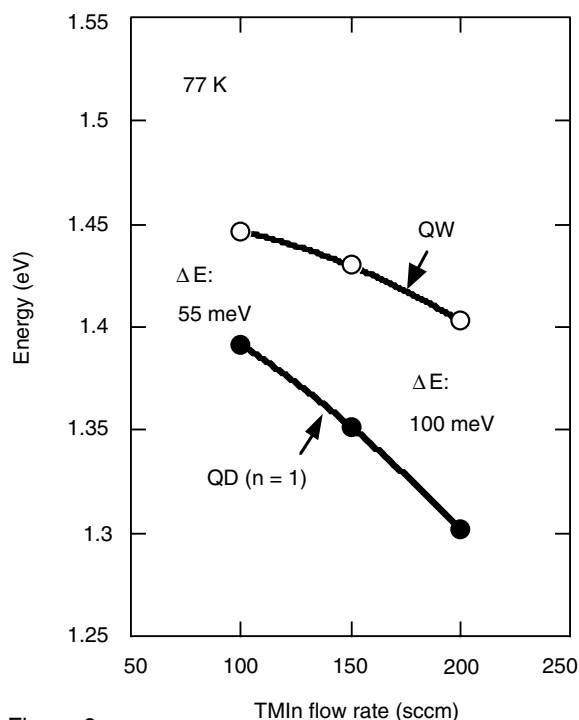


Figure 9 PL emission energy at 77 K as function of TMIn flow rates during growth.

In this section, we show that the TSR is a versatile structure for achieving flexible control of the QDs.

**Figure 9** shows the change of PL energies of the QD ground state and the QW at 77 K as a function of the TMIn flow rates. In this case, the nominal InGaAs thickness,  $L_w$ , was fixed at 5 nm. Both peaks shift to the lower energy side with an increasing TMIn flow rate owing to the increased In composition in QDs and QWs. This indicates that we can control the energy levels of QDs by changing the gas-phase composition during InGaAs growth. The energy difference,  $\Delta E$ , between the QW and QD changes from 55 meV to 100 meV when the TMIn flow rate is changed from 100 sccm to 200 sccm. This means that the incorporation of In atoms is more enhanced in QDs than in QWs; the difference here is probably related to the different InGaAs growth kinetics between the (111)B bottom and {111}A side faces. Note that the In-rich TSR-QD is sandwiched by GaAs in the perpendicular direction and is surrounded by the In-poor InGaAs QWs in the horizontal direction.

Therefore, the results imply that increasing the In content in the InGaAs layer enhances the strength of zero-dimensional carrier confinement in the TSR-QDs not only in the vertical direction but also in the horizontal direction.

Next, we changed the InGaAs growth thickness while maintaining the TMIIn flow rate at 100 sccm. We can control the size of the In-rich dot in the vertical direction simply by changing the InGaAs growth time. From the geometrical relationship, the height of the TSR-QD,  $h_d$ , is given by:

$$h_d = \frac{L_w}{\cos\theta} = 3L_w \quad (4),$$

where  $L_w$  is the width of the InGaAs QW at {111}A and  $\theta$  is the angle between the [111]A vector and <111>B vector and is about 70.5°. Therefore, in the case of a thick  $L_w$ , the In-rich region at the bottom will become an elongated QD, in other

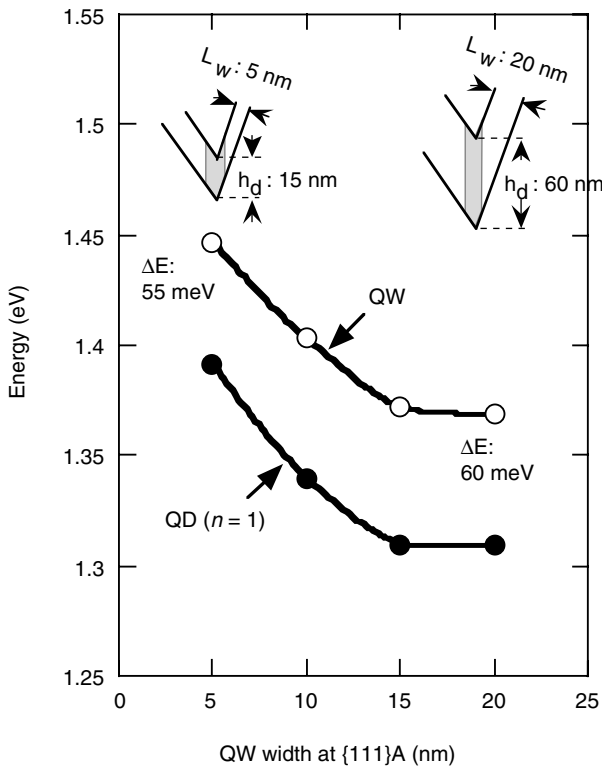


Figure 10  
PL emission energy at 77 K as a function of InGaAs growth thickness on {111}A faces.

words, a quantum dash or a quantum wire (see the inset in Figure 10). **Figure 10** shows the variation of PL energy positions of the QDs at the ground state and the QWs at 77 K as a function of  $L_w$ . As expected, the PL energy of the QWs shifts toward the lower energy side with an increasing  $L_w$ , and the quantum size effect is observed when  $L_w$  is less than 15 nm. The QDs and QWs show a similar PL energy dependence on  $L_w$  ( $= 1/3 h_d$ ). Hence, the energy level of the QD ground state can be artificially controlled by changing the vertical length of the TSR-QDs.

As stated above, by growing the quantum structures inside the TSRs, we can independently control the height and indium content of the dot. This is one of the big advantages of the TSR structures over the self-assembled technique governed by the S-K growth mode, where there is an inseparable correlation between the size and composition of the dot.<sup>30</sup> In addition, although no data are shown here, we have verified that the changes in the strength of the QD confinement potential and its anisotropy between the vertical and horizontal directions, which can be deduced from the magneto-PL results, are consistent with the intentional structural changes that the various growth conditions were designed to produce. Details are reported elsewhere.<sup>31)</sup>

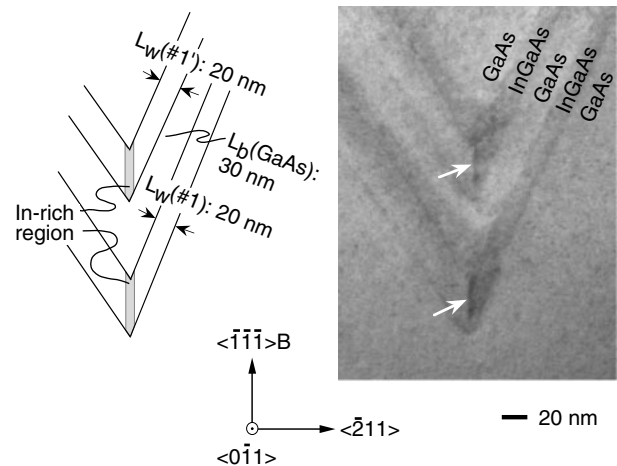


Figure 11  
Cross-sectional TEM image of double-stacked TSR-QDs. Arrows indicate positions of dots.

Another important feature is that the dots can easily be stacked. Stacking is attractive, particularly from the device applications point of view, because it enables us not only to increase the density of the dots but also to create quantum mechanical tunneling structures through QDs.<sup>32)-34)</sup> **Figure 11** shows a cross-sectional TEM image of double-stacked TSR-QDs. We grew 20 nm-thick double InGaAs layers under a TMI<sub>n</sub> flow rate of 100 sccm on both sides of a 30 nm-thick GaAs intermediate layer so that we could easily observe the structures that are grown. The two dots are the same size and are precisely aligned with each other in the vertical direction, proving that the TSR technology is suitable for realizing such a structure.

We studied the stacked structures using the conventional PL technique. **Figure 12(a)** shows the 77 K PL spectra obtained from the three structures shown in Figure 12(b). These structures are a single TSR-QD (A) ( $L_w = 5$  nm), a stack of two identical dots (AA), and a stack of two TSR-QDs of different sizes (AB) ( $L_w = 5$  nm and 10 nm). Sample AA has almost the same spectral shape as A, whereas sample AB shows two distinct QD peaks. Since the position of the higher energy peak

coincides with the QD peak of A, the lower peak is from the larger dot. Moreover, sample AB has a very weak peak at 1.43 eV, which is from the 10 nm-thick QW. There is no observable peak for the 5 nm-thick QW of sample AB because the recombination probability at that QW is much lower than the recombination probability at the 10 nm-thick QW. These results clearly prove the excellent growth controllability of QD stacking in TSR structures.

### 3. Electron Transport Studies and Device Applications

Many methods have been proposed and demonstrated for novel devices that incorporate semiconductor QDs. In particular, a great deal of effort has been devoted to fabricating self-assembled QD lasers<sup>35),36)</sup> because they are theoretically predicted to exhibit optical properties superior to those of conventional QW lasers, for example, a lower threshold current density and better temperature characteristics.<sup>9),37)</sup> However, our aim is to fabricate an integrated circuit consisting of a large number of ultra-small electronic memory devices using TSR-QDs. As explained in the previous section, TSR-QDs have several technological advantages in the fabrication of electronic devices. We have two kinds of strategies for realizing memory devices. One is to use resonant tunneling structures through multiple quantum dots since it is believed that the inherent bistability of voltage at the node between two sets of a dot and tunnel barriers can provide a memory action. The other is to use a nonvolatile field effect transistor (FET) with a QD charge-trapping floating gate, similar to the metal-oxide-semiconductor (MOS) FET with a nanoscale floating gate.<sup>7),8)</sup> Here, we explain the present stage of research on these devices.

#### 3.1 Resonant tunneling device

The transport of electrons through zero-dimensional QDs has been extensively studied, highlighting both the resonant tunneling (quantum

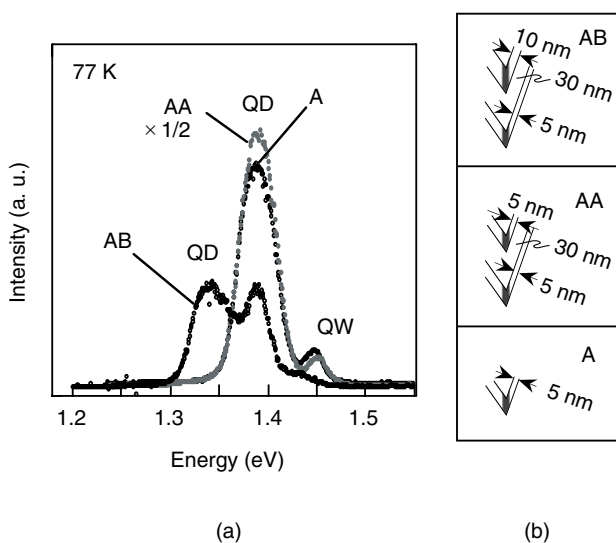


Figure 12  
(a) PL spectra of three kinds of structures grown on TSRs, and (b) the corresponding growth structures.

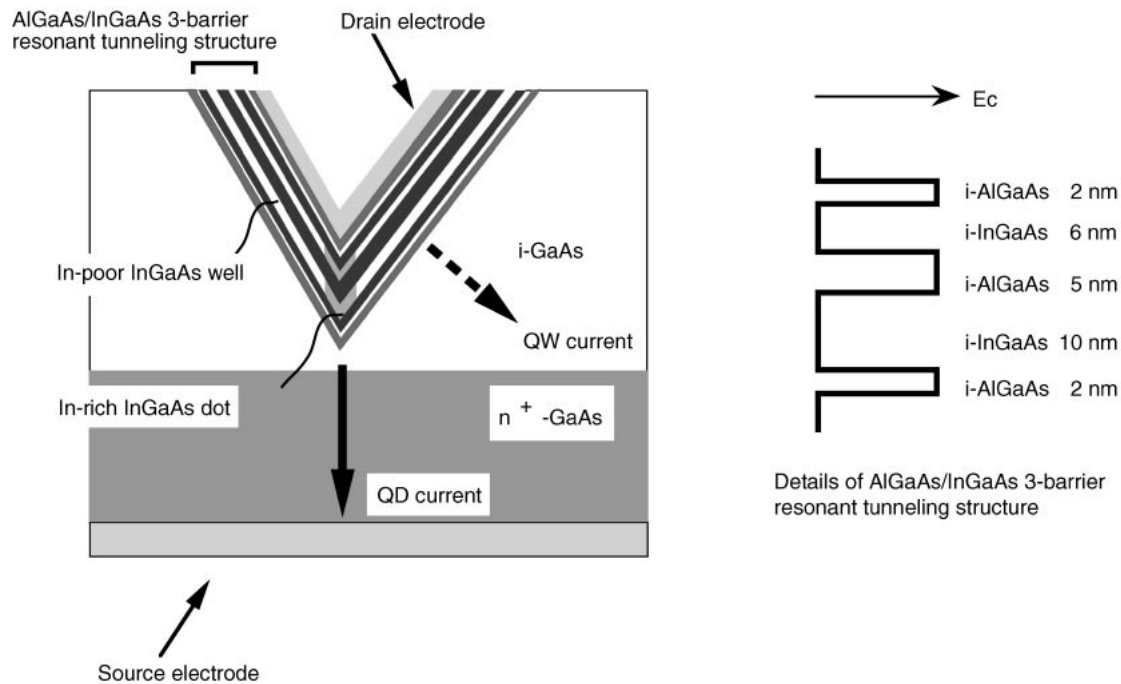


Figure 13  
Double-stacked TSR-QD diode for measuring I-V characteristic.

effects) and the single-electron charging phenomena (Coulomb effects).<sup>38)-44)</sup> In particular, for resonant tunneling, there has been the prediction that a high peak-to-valley (P/V) current ratio will be attained in the negative differential resistance (NDR) region of the diode current-voltage (I-V) characteristics if resonant tunneling occurs between at least two QDs.<sup>45)</sup> This is based on the expectation that inelastic phonon scattering of the tunneling electrons is suppressed due to the discreteness of the atom-like density of states in a QD, hence leading to an extremely small excess current at the valley region of the NDR characteristics. More precisely, it has been claimed that the energy relaxation of carriers is restricted to a narrow energy regime where the energy spacing between the QD subbands exactly matches the LO-phonon energy of the QD material.<sup>46),47)</sup> This is often called the phonon-bottleneck problem.<sup>46),47)</sup> It was further proposed that, if one substitutes QDs for the conventional 2D QWs of the double-emitter resonant-tunneling hot-electron transistor (DE-RHET), which provides a static random

access memory (SRAM) operation by itself,<sup>48)</sup> the power consumption would be drastically lowered.<sup>45)</sup> The phonon-bottleneck in energy relaxation of carriers was experimentally confirmed in the I-V characteristics of magnetically-confined, quasi zero-dimensional  $\text{In}_{0.53}\text{Ga}_{0.47}\text{As}/\text{In}_{0.52}\text{Al}_{0.48}\text{As}$  triple-barrier resonant tunneling diodes (RTDs).<sup>49),50)</sup> Under the application of high-intensity magnetic fields perpendicular to the heterointerfaces, the excess valley current was reduced and the P/V ratio was increased up to as high as 125 at low temperature.<sup>50)</sup> Therefore, if a similar result is achieved in a structurally-confined real QD system, we can obtain an SRAM having an extremely low power consumption and an ultra-small size.

Before making the device structures, we needed to investigate the electron transport through the TSR-QD. To do this, we fabricated the double-stacked TSR-QD structure shown in **Figure 13**.<sup>51)</sup> First, we formed TSRs in an undoped-GaAs layer which was previously grown on a Si-doped  $n^+$  (111)B GaAs substrate. Then, we

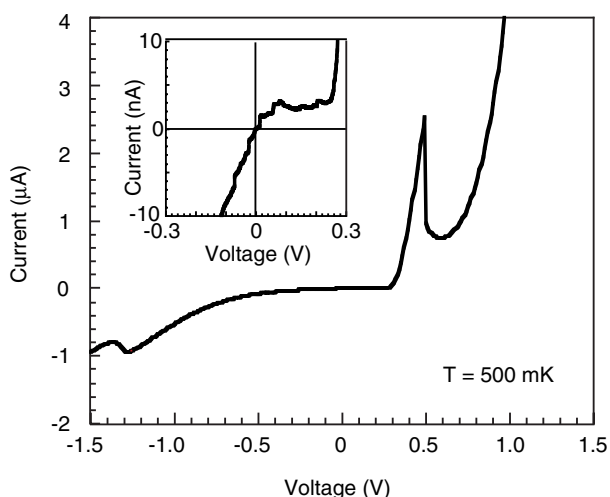


Figure 14 I-V characteristic of diode at 500 mK. Inset shows existence of fine structures at low bias.

grew Se-doped  $n^+$ -GaAs/InGaAs buffer layers, an undoped AlGaAs/InGaAs triple-barrier resonant tunneling structure, and  $n^+$ -GaAs/InGaAs for ohmic contact layers. The composition of AlGaAs and InGaAs and the concentration of Se doping were controllable, but their absolute values in our experiments are unknown. The electrodes were formed by evaporating AuGe/Au layers on the top and rear of the sample. The growth and device fabrication, including the ohmic contact to the top

surface, were done without removing the  $\text{SiO}_2$  mask that was initially used to form the TSRs (this mask had round openings). This allowed us to make a sample that permits measurement of the electronic property of an individual TSR structure in a self-aligned manner. Since we intended to primarily measure the transport property through the vertically-aligned QDs by suppressing the current flows through the TSR side surfaces, the bottoms of the TSRs were initially set close to the interface between the undoped GaAs and  $n^+$  substrate so that the electric field was concentrated on the dots.

**Figure 14** shows the I-V characteristics at 500 mK of a structure grown on a single TSR. NDRs in the  $\mu\text{A}$  range were observed under positive and negative biases. Fine nA structures were observed in the lower bias region, as shown in the inset. Currently, we are speculating that the NDRs at the higher bias and the fine structures at the lower bias are due to resonant tunneling through the QWs at the sidewalls and through the QDs at the bottom, respectively.

Looking more closely at the lower bias region, a steep rise followed by a gradual decrease in the current was observed at several voltages in the

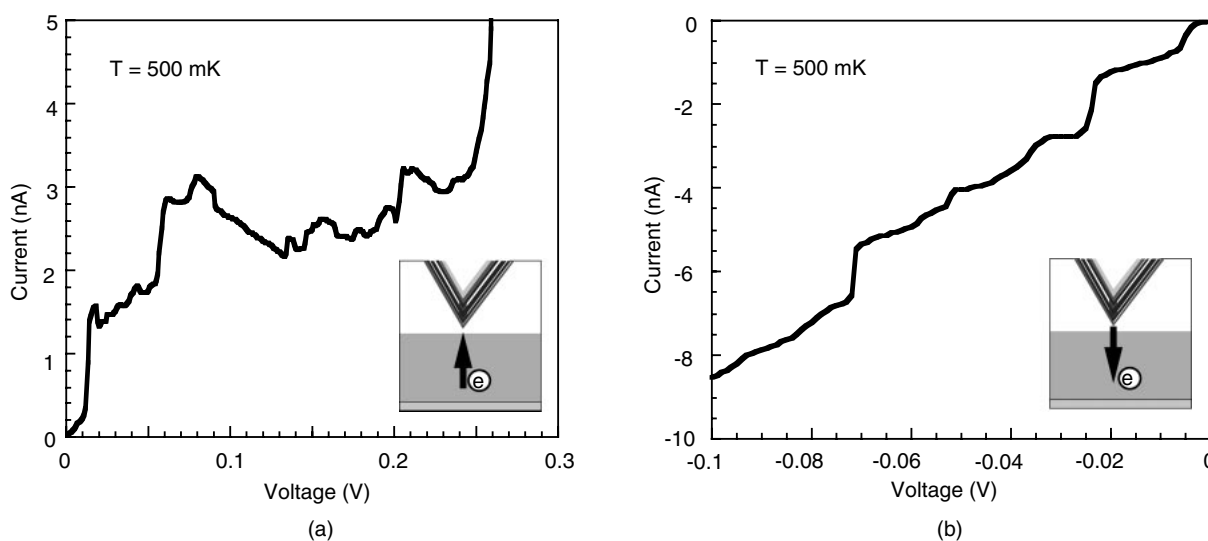


Figure 15 Enlarged sections of I-V characteristic at low bias. (a) Positive side, and (b) negative side.

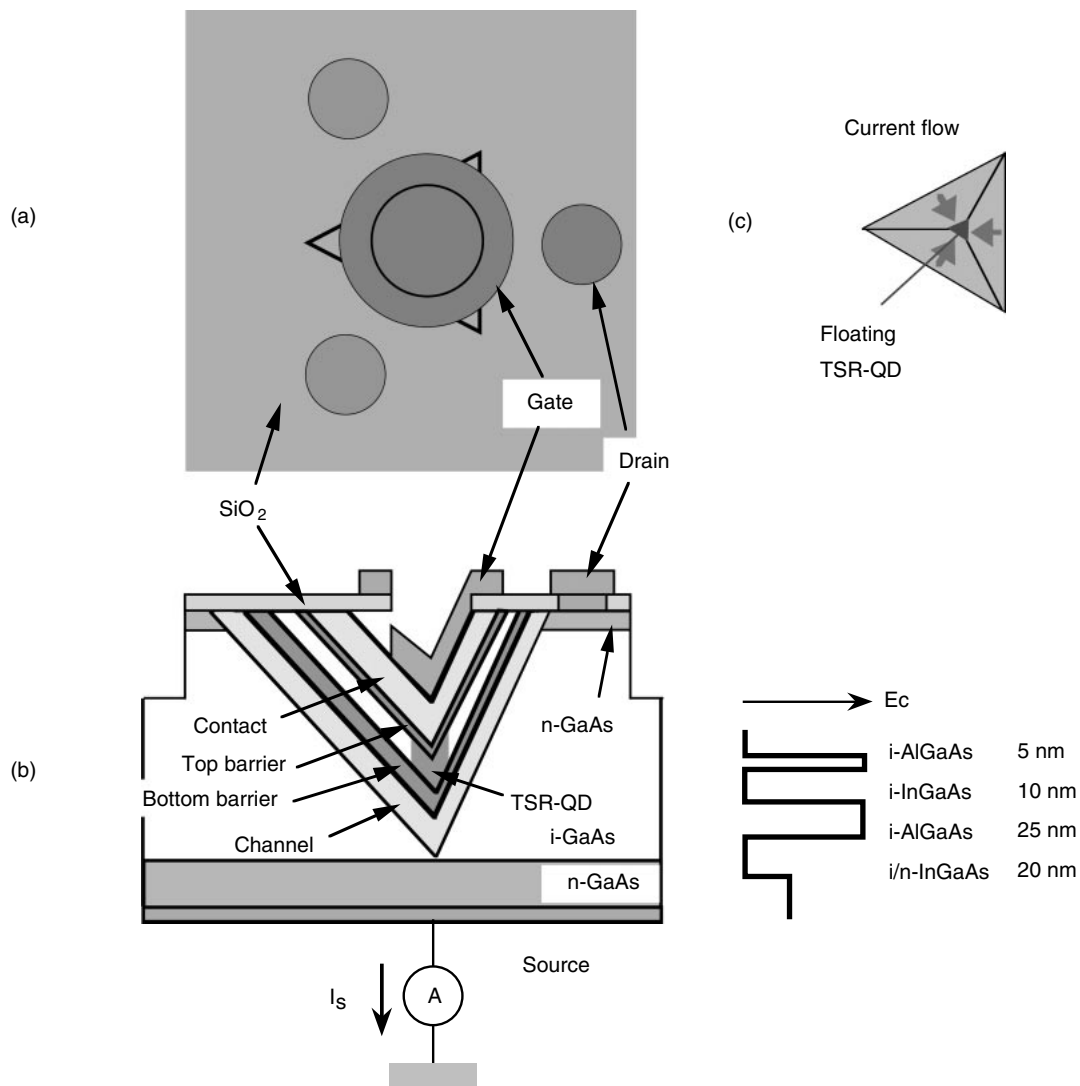


Figure 16 Novel doped-channel FET with buried gate consisting of floating TSR-QD. (a) Top view, (b) side view, and (c) current flow at sidewalls.

positive region [Figure 15(a)]. According to the theoretical calculation by Bryant,<sup>52)</sup> this peculiar I-V characteristic is a typical feature of a system containing double dots which are strongly coupled to each other in a quantum mechanical sense. On the other hand, as shown in Figure 15(b), no NDRs other than staircases were observed on the negative bias side of the I-V curve. Unfortunately, we have not yet obtained the expected large P/V ratio in the TSR-QD diodes. To more deeply understand the mechanism of electron transport through TSR-QDs, we have to investigate more growth structures in the TSR and optimize them.

### 3.2 Charge trapping device

Another possibility for using the TSR-QDs to make a memory device is a nonvolatile InGaAs/AlGaAs doped-channel heterostructure FET in which an electrically floating, In-rich InGaAs TSR-QD is placed between the electron channel and the gate electrode. Figure 16 shows a schematic of the device structure. Prior to the TSR formation, we prepared the planar substrate by forming a thick, undoped GaAs layer on a Si-doped n<sup>+</sup>(111)B GaAs followed by a 75 nm-thick Se-doped n<sup>+</sup>-GaAs layer on the surface using MOCVD at 800°C. After forming TSRs in the wet etching pro-

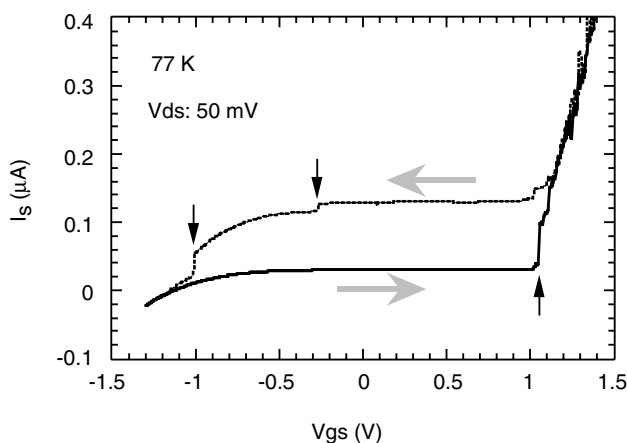


Figure 17  
Measured  $V_{gs}$ - $I_s$  characteristic at 77 K.

cess so that the apexes of the TSRs did not reach to the undoped GaAs layer, we grew Se-doped  $n^+$ -GaAs/InGaAs layers, an undoped AlGaAs (25 nm)/InGaAs (10 nm)/AlGaAs (5 nm) double-barrier structure, and Se-doped  $n^+$ -GaAs/InGaAs inside the TSRs, again using MOCVD. In this structure, the buried  $n^+$ -InGaAs layer at the sidewalls acts as a doped channel for electrons. The source was  $n^+$ -substrate and the drain was surface  $n^+$ -GaAs. The gate electrode was formed on the  $n^+$ -InGaAs at the topmost surface in the TSR by evaporating AuGe/Au without alloying. The  $\text{SiO}_2$  mask remained in place throughout the growth and device fabrication process. Since an In-rich InGaAs-QD is self-formed at the bottom of a TSR, we expect that the trapping and detrapping of electrons from the gate electrode can be controlled by using a thin, top AlGaAs tunnel barrier.

**Figure 17** shows how the source current,  $I_s$ , changes with the gate voltage,  $V_{gs}$ , for a single TSR structure at 77 K. Here, a constant  $V_{ds}$  of 50 mV was applied between the source and drain electrodes. We found a clear hysteresis in the  $V_{gs}$ - $I_s$  characteristics. We believe that this bistability of  $I_s$  is due either to the state when the TSR-QD has few electrons or when it has many electrons. The lower curve might correspond to the many-electron state, and the upper curve might correspond to the few-electron state. When we changed  $V_{gs}$

from -1.3 V to 1.1 V, there was no significant increase in  $I_s$ . However, at  $V_{gs} = 1.1$  V,  $I_s$  increased in a step-like manner, probably due to the escape of some of the captured electrons from the TSR-QD by tunneling to the gate electrode through the thin AlGaAs barrier. The steep increase in  $I_s$  beyond  $V_{gs} = 1.1$  V might be caused by the increase in the number of electrons injected from the source to the FET channel in the vicinity of the initial TSR bottom due to the positive gate voltage. When we decreased  $V_{gs}$  from 1.1 V to -1.0 V, we observed a larger  $I_s$  than in the many-electron-state part of the lower curve because the TSR-QD remained in the few-electron state. At  $V_{gs} = -1.0$  V, the TSR-QD might be charged by electrons that tunnel through the AlGaAs barrier from the gate electrode. As a result, the  $I_s$  transits to a part of the lower curve where the dot is in the more-occupied state. The results shown in Figure 17 imply that we can program the  $I_s$  states around the low  $V_{gs}$  region by charging or discharging the TSR-QD using the gate electrode.

We have observed a memory action in our novel FET structure, in which a TSR-QD is placed between the channel and the gate electrode. However, these are just phenomenological observations. Although a nonvolatile memory effect is expected, the retention time seems to be less than a hour at 77 K. Considering the principle of device operation, we speculate that the height of the potential barrier at the undoped GaAs between the apex of the TSR and the  $n^+$  substrate (source) is strongly affected by the number of occupied electrons in the TSR-QD, and that most of the FET current will be passed by way of the apex region to the  $n^+$  substrate. If the TSR-QD is charged by many electrons, electron injection from the source to the doped channel at the TSR apex will be hindered by the increased height of the potential barrier. Therefore, the current flow through the FET channel will remain small without a large positive  $V_{gs}$ . However, when the TSR-QD has only a few electrons, the barrier height will be low and the electron flow from source to drain will be high-

er. Thus, the two types of potential profiles near the apex of the TSR will introduce a memory effect in the  $I_s$ - $V_{gs}$  characteristics. However, much work remains to be done before the mechanism of device operation, including the memory effect, becomes clear.

#### 4. Conclusion

This paper described our original QD structures formed in tetrahedral-shaped recesses (TSRs) on (111)B-oriented GaAs substrates. We reviewed these TSR-QDs in detail from the viewpoints of material science and device application.

First, we explained the fabrication procedure for InGaAs QDs in TSRs using MOCVD. We performed low-temperature PL and CL studies on TSR samples in which a GaAs/InGaAs/GaAs heterostructure was grown and showed that there are two distinct PL peaks. From CL mapping experiments, we found that the higher-energy emission is from the sidewalls of the TSR and the lower-energy emission is from the bottom. In addition, we found that the intensity of the luminescence peak from the bottom clearly exhibited band-filling as the excitation power was increased, while that from the sidewalls showed no filling effect. These results strongly imply the formation of QDs at the bottom of the TSRs and QWs at the side surfaces.

Then, structural analyses by cross-sectional TEM and EDX clarified that an InGaAs nanostructure with a higher In composition than that of the sidewall InGaAs QWs was spontaneously grown at the TSR bottom region, which is in good agreement with the PL and CL data. To elucidate the self-forming mechanism of TSR-QDs, we proposed a growth model having a non-uniform InGaAs composition in the TSR based on the possibility that the composition might be strongly affected by the local crystallographic orientations inside the TSR. To test the model, we studied the chemical composition of InGaAs layers grown on (100), (111)A, and (111)B GaAs planar substrates

using AES. As a result, we found that the In composition of the InGaAs is clearly the highest on a (111)B substrate. This proves that InGaAs growth is kinetically controlled under the employed growth conditions, leading to different In compositions among substrates of different orientations. Based on this result, we explained that In-rich InGaAs is grown in a self-forming manner at the TSR bottom because the bottom region has a (111)B-like bond configuration.

Furthermore, to obtain more direct evidence of QD formation and obtain knowledge of the horizontal extent of the wavefunction of the confined carriers, we performed magneto-PL studies on our sample. The PL properties under a magnetic field showed zero-dimensional behavior, proving that the carriers are actually confined at the bottom of the TSR.

Then, we presented the results of experiments which indicated that we can control the energy levels and the strength of carrier confinement potential in TSR-QDs by independently changing the In content and the thickness of InGaAs during MOCVD growth. TEM and PL results confirmed that we can stack the TSR-QDs precisely in the vertical direction and can independently control the height of each TSR. From these results, we concluded that the TSR is a versatile structure for flexibly controlling QDs and applying them to practical electronic devices.

Lastly, for the application of TSR-QDs in electronic memory devices, we introduced two structures: a resonant tunneling diode having double-stacked TSRs, and a novel heterostructure FET with a floating TSR-QD above part of the channel. In the double-stacked TSR-QD diode, we observed the I-V characteristics that are peculiar to resonant tunneling through a strongly coupled two-dot system at low temperature. Although we expected to be able to observe an increased P/V current ratio in the zero-dimensional RTD and apply the results to make a low-power SRAM, our current level of research is insufficient to meet

these expectations. However, we have observed nonvolatile, bistable  $V_{gs}$ - $I_s$  characteristics in a novel doped-channel InGaAs/AlGaAs FET in which a TSR-QD is placed between the channel and the gate electrode. We explained that the bistability might originate from the charged or discharged state of the buried TSR-QD and that the state can be programmed by tunneling electrons through the AlGaAs barrier from the gate electrode.

### Acknowledgments

This work was performed under the management of FED as part of the MITI R&D program (Quantum Functional Device Project) supported by NEDO.

The authors would like to thank Dr. H. Ishikawa and Dr. N. Yokoyama for their strong support and encouragement throughout this work.

We would like to thank Professor N. Miura and Dr. K. Uchida at ISSP, the University of Tokyo for their assistance in the magneto-PL experiments and fruitful discussion. We would also like to thank Dr. T. Sekiguchi at IMR of Tohoku University for his help in the CL experiments and equally valuable advice.

### References

- 1) H. Sakaki: Scattering Suppression and High-Mobility Effect of Size-Quantized Electrons in Ultrafine Semiconductor Wire Structures. *Jpn. J. Appl. Phys.*, **19**, 12, pp.L735-L738 (1980).
- 2) E. Kapon, D. M. Hwang, and R. Bhat: Stimulated Emission in Semiconductor Quantum Wire Heterostructures. *Phys. Rev. Lett.*, **63**, 4, pp.430-433 (1989).
- 3) T. Fukui, S. Ando, Y. Tokura, and T. Toriyama: GaAs Tetrahedral Quantum Dot Structures Fabricated Using Selective Area Metalorganic Chemical Vapor Deposition. *Appl. Phys. Lett.*, **58**, 18, pp.2018-2020 (1991).
- 4) S. Tsukamoto, Y. Nagamune, M. Nishioka, and Y. Arakawa: Fabrication of GaAs Quantum Wires on Epitaxially Grown V Grooves by Metal-Organic Chemical-Vapor Deposition. *J. Appl. Phys.*, **71**, 1, pp.533-535 (1992).
- 5) K. Yano, T. Ishii, T. Hashimoto, T. Kobayashi, F. Murai, and K. Seki: Room-Temperature Single-Electron Memory. *IEEE Trans. Electron Devices*, **41**, 9, pp.1628-1638 (1994).
- 6) S. Tiwari, F. Rana, H. Hanafi, A. Hartstein, E. F. Crabbé, and K. Chan: A Silicon Nanocrystals Based Memory. *Appl. Phys. Lett.*, **68**, 10, pp.1377-1379 (1996).
- 7) L. Guo, E. Leobandung, and S. Y. Chou: A Room-Temperature Silicon Single-Electron Metal-Oxide-Semiconductor Memory with Nanoscale Floating-Gate and Ultranarrow Channel. *Appl. Phys. Lett.*, **70**, 7, pp.850-852 (1997).
- 8) A. Nakajima, T. Futatsugi, K. Kosemura, T. Fukano, and N. Yokoyama: Room Temperature Operation of Si Single-Electron Memory with Self-Aligned Floating Dot Gate. *Appl. Phys. Lett.*, **70**, 13, pp.1742-1744 (1997).
- 9) Y. Arakawa and H. Sakaki: Multidimensional Quantum Well Laser and Temperature Dependence of Its Threshold Current. *Appl. Phys. Lett.*, **40**, 11, pp.939-941 (1982).
- 10) M. A. Reed, R. T. Bate, K. Bradshaw, W. M. Duncan, W. R. Frensley, J. W. Lee, and H. D. Shih: Spatial Quantization in GaAs-AlGaAs Multiple Quantum Dots. *J. Vac. Sci. Technol.*, **B4**, 1, pp.358-360 (1986).
- 11) Y. D. Galeuchet, H. Rothuizen, and P. Roentgen: In Situ Buried GaInAs/InP Quantum Dot Arrays by Selective Area Metalorganic Vapor Phase Epitaxy. *Appl. Phys. Lett.*, **58**, 21, pp.2423-2425 (1991).
- 12) Y. Nagamune, M. Nishioka, S. Tsukamoto, and Y. Arakawa: GaAs Quantum Dots with Lateral Dimension of 25 nm Fabricated by Selective Metalorganic Chemical Vapor Deposition Growth. *Appl. Phys. Lett.*, **64**, 19, pp.2495-2497 (1994).
- 13) K. C. Rajkumar, A. Madhukar, K. Rammohan, D. H. Rich, P. Chen, and L. Chen: Optically Active Three-Dimensionally Confined Struc-

- tures Realized via Molecular Beam Epitaxial Growth on Nonplanar GaAs (111)B. *Appl. Phys. Lett.*, **63**, 21, pp.2905-2907 (1993).
- 14) M. Tabuchi, S. Noda, and A. Sasaki: Mesoscopic Structure in Lattice-Mismatched Heteroepitaxial Interface Layers. *Science and Technology of Mesoscopic Structures*, S. Namba, C. Hamaguchi, and T. Ando ed., Tokyo, Springer-Verlag, 1992, pp. 379-384.
  - 15) D. Leonard, M. Krishnamurthy, C. M. Reeves, S. P. Denbaars, and P. M. Petroff: Direct Formation of Quantum-Sized Dots from Uniform Coherent Islands of InGaAs on GaAs Surfaces. *Appl. Phys. Lett.*, **63**, 23, pp.3203-3205 (1993).
  - 16) J. M. Moison, F. Houzay, F. Barthe, L. Leprince, E. André, and O. Vatel: Self-Organized Growth of Regular Nanometer-Scale InAs Dots on GaAs. *Appl. Phys. Lett.*, **64**, 2, pp.196-198 (1994).
  - 17) Y. Sakuma, Y. Sugiyama, S. Muto, and N. Yokoyama: A New Approach to AlAs/GaAs Quantum Dot Structures Using MOVPE on Tetrahedral-Shaped Recesses Formed on (111)B GaAs Substrates. presented at *21st International Symposium on Compound Semiconductors*, San Diego, 1994.
  - 18) Y. Sugiyama, Y. Sakuma, S. Muto, and N. Yokoyama: Novel InGaAs/GaAs Quantum Dot Structures Formed in Tetrahedral-Shaped Recesses on (111)B GaAs Substrates Using Metalorganic Vapor Phase Epitaxy. *Appl. Phys. Lett.*, **67**, 2, pp.256-258 (1995).
  - 19) Y. Tarui, Y. Komiya, and Y. Harada: Preferential Etching and Etched Profile of GaAs. *J. Electrochem. Soc.*, **118**, 1, pp.118-122 (1971).
  - 20) X. L. Wang, M. Ogura, and H. Matsuhata: Flow Rate Modulation Epitaxy of AlGaAs/GaAs Quantum Wires on Nonplanar Substrate. *Appl. Phys. Lett.*, **66**, 12, pp.1506-1508 (1995).
  - 21) T. Sekiguchi, Y. Sakuma, Y. Awano, and N. Yokoyama: Cathodoluminescence Study of InGaAs/GaAs Quantum Dot Structures Formed on The Tetrahedral-Shaped Recesses on GaAs (111)B Substrates. *J. Appl. Phys.* **83**, 9, pp.4944-4950 (1998).
  - 22) O. Kayser: Selective Growth of InP/GaInAs in LP-MOVPE and MOMBE/CBE. *J. Cryst. Growth*, **107**, pp.989-998 (1991).
  - 23) B. P. Keller, S. Keller, H. Herrnberger, J. Lenzner, S. Nilsson, and W. Seifert: Compositional Gradients in Ga<sub>x</sub>In<sub>1-x</sub>As on Patterned InP Substrates Grown by Atmospheric-Pressure Metalorganic Vapour Phase Epitaxy. *J. Cryst. Growth*, **140**, pp.33-40 (1994).
  - 24) M. Y. Yen and T. W. Haas: Dynamics of Reflection High-Energy Electron Diffraction Intensity Oscillations during Molecular Beam Epitaxial Growth of GaAs on (111)B GaAs Substrates. *Appl. Phys. Lett.*, **56**, 25, pp.2533-2535 (1990).
  - 25) K. Kamon, M. Shimazu, K. Kimura, M. Mihara, and M. Ishii: Orientation Dependence of GaAs Growth in Low-Pressure MOVPE. *J. Cryst. Growth*, **84**, pp.126-132 (1987).
  - 26) D. K. Biegelsen, R. D. Bringans, J. E. Northrup, and L. E. Swartz: Reconstructions of GaAs (111)B Surfaces Observed by Scanning Tunneling Microscopy. *Phys. Rev. Lett.*, **65**, 4, pp.452-455 (1990).
  - 27) O. Akimoto and H. Hasegawa: Interband Optical Transitions in Extremely Anisotropic Semiconductors. *J. Phys. Soc. Jpn.*, **22**, 1, pp.181-191 (1967).
  - 28) H. Q. Hou, W. Staguhn, N. Miura, Y. Segawa, S. Takeyama, Y. Aoyagi, and J. M. Zhou: Photoluminescence Intensity of InGaAs/GaAs Strained Quantum Wells under High Magnetic Fields. *Solid State Commun.*, **74**, 8, pp.687-691 (1990).
  - 29) Y. Nagamune, Y. Arakawa, S. Tsukamoto, M. Nishioka, S. Sasaki, and N. Miura: Photoluminescence Spectra and Anisotropic Energy Shift of GaAs Quantum Wires in High Magnetic Fields. *Phys. Rev. Lett.*, **69**, 20, pp.2963-2966 (1992).
  - 30) J. M. García, G. Medeiros-Ribeiro, K. Schmidt,

- T. Ngo, J. L. Feng, A. Lorke, J. Kotthaus, and P. M. Petroff: Intermixing and Shape Changes during The Formation of InAs Self-Assembled Quantum Dots. *Appl. Phys. Lett.*, **71**, 14, pp.2014-2016 (1997).
- 31) Y. Sakuma, Y. Awano, T. Futatsugi, N. Yokoyama, K. Uchida, and N. Miura: Magneto-Photoluminescence Study of Quantum Dots Formed on Tetrahedral-Shaped Recesses. *Solid-State Electron.*, **42**, 7-8, pp.1341-1347 (1998).
- 32) Q. Xie, A. Madhukar, P. Chen, and N. P. Kobayashi: Vertically Self-Organized InAs Quantum Box Islands on GaAs(100). *Phys. Rev. Lett.*, **75**, 13, pp.2542-2545 (1995).
- 33) G. S. Solomon, J. A. Trezza, A. F. Marshall, and J. S. Harris, Jr.: Vertically Aligned and Electronically Coupled Growth Induced InAs Islands in GaAs. *Phys. Rev. Lett.*, **76**, 6, pp.952-955 (1996).
- 34) M. S. Miller: Lateral Positioning and Vertical Stacking of InAs Islands on GaAs Substrates; Designing Quantum Transport Devices. *Jpn. J. Appl. Phys.*, **36**, Part 1-6B, pp.4123-4128 (1997).
- 35) N. Kirstaedter, N. N. Ledentsov, M. Grundmann, D. Bimberg, V. M. Ustinov, S. S. Ruvimov, M. V. Maximov, P. S. Kop'ev, Zh. I. Alferov, U. Richter, P. Werner, U. Gösele, and J. Heydenreich: Low Threshold, Large  $T_0$  Injection Laser Emission From (InGa)As Quantum Dots. *Electron. Lett.* **30**, 17, pp.1416-1417 (1994).
- 36) H. Shoji, Y. Nakata, K. Mukai, Y. Sugiyama, M. Sugawara, N. Yokoyama, and H. Ishikawa: Room Temperature CW Operation at The Ground State of Self-Formed Quantum Dot Lasers with Multi-Stacked Dot Layer. *Electron. Lett.* **32**, 21, pp.2023-2024 (1996).
- 37) M. Asada, Y. Miyamoto, and Y. Suematsu: Gain and The Threshold of Three-Dimensional Quantum-Box Lasers. *IEEE J. Quantum Electron.*, **QE-22**, 9, pp.1915-1921 (1986).
- 38) M. A. Reed, J. N. Randall, R. J. Aggarwal, R. J. Matyi, T. M. Moore, and A. E. Wetsel: Observation of Discrete Electronic States in A Zero-Dimensional Semiconductor Nanostructure. *Phys. Rev. Lett.*, **60**, 6, pp.535-537 (1988).
- 39) D. V. Averin, A. N. Korotkov, and K. K. Likharev: Theory of Single-Electron Charging of Quantum Wells and Dots. *Phys. Rev.*, **B44**, 12, pp.6199-6211 (1991).
- 40) M. Tewordt, L. Martín-Moreno, J. T. Nicholls, M. Pepper, M. J. Kelly, V. J. Law, D. A. Ritchie, J. E. F. Frost, and G. A. C. Jones: Single-Electron Tunneling and Coulomb Charging Effects in Asymmetric Double-Barrier Resonant-Tunneling Diodes. *Phys. Rev.*, **B45**, 24, pp.14407-14410 (1992).
- 41) D. G. Austing, T. Honda, Y. Tokura, and S. Tarucha: Sub-Micron Vertical AlGaAs/GaAs Resonant Tunneling Single Electron Transistor. *Jpn. J. Appl. Phys.*, **34**, Part 1-2B, pp.1320-1325 (1995).
- 42) I. E. Itskevich, T. Ihn, A. Thornton, M. Henini, T. J. Foster, P. Moriarty, A. Nogaret, P. H. Beton, L. Eaves, and P. C. Main: Resonant Magnetotunneling Through Individual Self-Assembled InAs Quantum Dots. *Phys. Rev.*, **B54**, 23, pp.16401-16404 (1996).
- 43) M. Narihiro, G. Yusa, Y. Nakamura, T. Noda, and H. Sakaki: Resonant Tunneling of Electrons via 20 nm Scale InAs Quantum Dot and Magnetotunneling Spectroscopy of Its Electronic States. *Appl. Phys. Lett.*, **70**, 1, pp.105-107 (1997).
- 44) T. Suzuki, K. Nomoto, K. Taira, and I. Hase: Tunneling Spectroscopy of InAs Wetting Layers and Self-Assembled Quantum Dots; Resonant Tunneling Through Two- and Zero-Dimensional Electronic States. *Jpn. J. Appl. Phys.*, **36**, Part 1-3B, pp.1917-1921 (1997).
- 45) Y. Awano, Y. Sakuma, Y. Sugiyama, C. Wirner, M. Takatsu, T. Mori, H. Nakao, M. Yamaguchi, M. Shima, and N. Yokoyama: Electrical and Optical Properties of Quantum Dot Structures; Magnetic-Confined and Tetrahedral-Shaped Recess (TSR) Quantum Dots. *Extended Abstracts of 15th Symposium on Future Electron Devices*, 1996, pp.46-51.

- 46) U. Bockelmann and G. Bastard: Phonon Scattering and Energy Relaxation in Two-, One, and Zero-Dimensional Electron Gases. *Phys. Rev.*, **B42**, 14, pp.8947-8951 (1990).
- 47) H. Benisty, C. M. Sotomayor-Torres, and C. Weisbuch: Intrinsic Mechanism for The Poor Luminescence Properties of Quantum-Box Systems. *Phys. Rev.* **B44**, 19, pp.10945-10948 (1991).
- 48) T. Mori, S. Muto, H. Tamura, and N. Yokoyama: A Static Random Access Memory Cell Using A Double-Emitter Resonant-Tunneling Hot Electron Transistor for Gigabit-Plus Memory Applications. *Jpn. J. Appl. Phys.*, **33**, Part 1-1B, pp.790-793 (1994).
- 49) C. Wirner, Y. Awano, T. Futatsugi, N. Yokoyama, T. Nakagawa, H. Bando, S. Muto, M. Ohno, and N. Miura: Phonon Assisted Tunneling and Peak-to-Valley Ratio in A Magnetically Confined Quasi Zero Dimensional InGaAs/InAlAs Resonant Tunneling Diode. *Jpn. J. Appl. Phys.*, **36**, Part 1-3B, pp.1958-1960 (1997).
- 50) C. Wirner, Y. Awano, N. Yokoyama, M. Ohno, N. Miura, T. Nakagawa, and H. Bando: Phonon Bottleneck Effects in An InGaAs/InAlAs Triple Barrier Tunneling Diode at High Magnetic Fields. *Semicond. Sci. Technol.*, **12**, pp.998-1002 (1997).
- 51) M. Shima, Y. Sakuma, C. Wirner, T. Strutz, E. Taguchi, T. Futatsugi, Y. Awano, and N. Yokoyama: Electron Transport Through Tetrahedral-Shaped Recess (TSR) Stacked Double Quantum Dot Structures. *1997 IEEE International Symposium on Compound Semiconductors*, M. Melloch and M. A. Reed ed., San Diego, Institute of Physics Publishing, 1997, pp.539-542.
- 52) G. W. Bryant: Resonant Tunneling Through Coupled, Double-Quantum-Box Nanostructures. *Phys. Rev.*, **B44**, 7, pp.3064-3069 (1991).



**Yoshiki Sakuma** received the B.E. and M.E. degrees in Electronic Engineering from Tohoku University, Sendai, Japan in 1985 and 1987, respectively, and the Ph.D. degree in Materials Physics from Osaka University, Osaka, Japan in 1997. He joined Fujitsu Laboratories Ltd., Atsugi, Japan in 1987, where he has been engaged in research on atomic layer epitaxy of III-V compound semiconductors. His current interests include

developing novel methods for fabricating semiconductor nanostructures. He is a member of the Japan Society of Applied Physics.



**Yuji Awano** received the B.E., M.E., and Ph. D. degrees in Electronic Engineering from Meiji University, Tokyo, Japan in 1980, 1982, and 1985, respectively. He joined Fujitsu Laboratories Ltd., Atsugi, Japan in 1985, where he has been working on theoretical and experimental research of very short gate HEMTs. He is currently a senior researcher at the Quantum Electron Device laboratory and is responsible for

the research and development of quantum dot electron devices and sub-0.1 micron FETs. He is a member of the Japan Society of Applied Physics, the Institute of Electronics, Information and Communication Engineers, and the IEEE Electron Device Society.



**Masashi Shima** received the B.E. degree in Mechanical Engineering from Waseda University, Tokyo, Japan in 1989 and the M.S. degree in Materials Science and Engineering from Tokyo Institute of Technology, Tokyo, Japan in 1991.

He joined Fujitsu Laboratories Ltd., Atsugi, Japan in 1991, where he has been engaged in the research and development of short-gate HEMTs. He is currently developing quantum effect devices utilizing quantum dots. He is a member of the Japan Society of Applied Physics.